CHEMISTRY
A EUROPEAN JOURNAL

DOI: 10.1002/chem.200601772

$Sn_{20.5}\square_{3.5}As_{22}I_8$: A Largely Disordered Cationic Clathrate with a New Type of Superstructure and Abnormally Low Thermal Conductivity

Julia V. Zaikina,[a] Kirill A. Kovnir,[b] Alexei V. Sobolev,[c] Igor A. Presniakov,[c] Yuri Prots,[b] Michael Baitinger,[b] Walter Schnelle,[b] Andrei V. Olenev,[a] Oleg I. Lebedev,[d] Gustaaf Van Tendeloo,[d] Yuri Grin,[b] and Andrei V. Shevelkov*[a]

Abstract: $Sn_{20.5}As_{22}I_8$, a new cationic clathrate, has been prepared by using an ampoule technique. According to the X-ray powder diffraction data, it crystallizes in the face-centered cubic space group $F23$ or $Fm\bar{3}$ with a unit-cell parameter of $a = 22.1837(4)$ Å. Single-crystal X-ray data allowed solution of the crystal structure in the subcell with a unit-cell parameter of $a_0 = 11.092(1)$ Å and the space group $Pm\bar{3}n$ ($R = 5.7\,\%$). $Sn_{20.5}As_{22}I_8$ (or $Sn_{20.5}\square_{3.5}As_{22}I_8$, accounting for the vacancies in the framework) possesses the clathrate-I type crystal structure, with iodine atoms occupying the cages of the cationic framework composed of tin and arsenic atoms. The crystal structure is strongly disordered. The main features are a random distribution of vacancies, and shifts of the tin and arsenic atoms away from their ideal positions. The coordination of the tin atoms has been confirmed by using ^{119}Sn Mössbauer spectroscopy. Electron diffraction and high-resolution electron microscopy (HREM) analyses have confirmed the presence of the superstructure ordering, which results in a doubling of the unit-cell parameter and a change of the space group from $Pm\bar{3}n$ to either $F23$ or $Fm\bar{3}$. Analysis of the crystal structure has led to the construction of four ordering models for the superstructure, which have been corroborated by HREM, and has also led to the identification of disordered regions originating from overlap of the different types of ordered domains. $Sn_{20.5}As_{22}I_8$ is a diamagnetic semiconductor with an estimated band gap of 0.45 eV; it displays abnormally low thermal conductivity, with the room temperature value being just $0.5\ W\,m^{-1}\,K^{-1}$.

Keywords: clathrates · electron microscopy · superstructures · thermal conductivity · tin

Introduction

The search for new thermoelectric materials is motivated by the quest for an environmentally friendly and energy-saving approach to small-scale, solid-state refrigeration and/or power generation. An effective thermoelectric material should have a high electrical conductivity (σ), a large Seebeck coefficient (S), and simultaneously possess low thermal conductivity (κ) such that the dimensionless figure of merit ($ZT = S^2T\sigma/\kappa$) considerably exceeds unity. The "phonon glass, electron crystal" (PGEC) concept introduced by Slack[1] identifies the range of crystal structures potentially relevant for thermoelectric cooling purposes, such as cage-like structures incorporating loosely bound guest atoms. In such structures, the guest atoms are trapped inside oversized cages and may "rattle", leading to a suppression of thermal conductivity due to effective phonon scattering, without impeding the transport of charge carriers. Filled skutterudites,[2] as well as intermetallic clathrates and clathrate-like compounds,[3] are considered to conform to the PGEC con-

[a] Dipl.-Chem. J. V. Zaikina, Dr. A. V. Olenev, Prof. Dr. A. V. Shevelkov
Inorganic Synthesis Laboratory, Department of Chemistry
Moscow State University
119992 Moscow (Russia)
Fax: (+7) 495-939-4788
E-mail: shev@inorg.chem.msu.ru

[b] Dr. K. A. Kovnir, Dr. Yu. Prots, Dr. M. Baitinger, Dr. W. Schnelle, Prof. Dr. Yu. Grin
Max-Planck-Institut für Chemische Physik fester Stoffe
01187 Dresden (Germany)

[c] Dr. A. V. Sobolev, Dr. I. A. Presniakov
Chair of Radiochemistry, Moscow State University
119992 Moscow (Russia)

[d] Dr. O. I. Lebedev, Prof. Dr. G. Van Tendeloo
EMAT, University of Antwerp
2020 Antwerpen, Belgium

cept, and recent investigations of their physical properties[4,5] have confirmed these classes of compounds to be prospective thermoelectric materials. Intermetallic clathrates of the type A_8T_{46-y} (A = alkali metal; T = a tetrel, i.e., a group 14 element),[6] in which three-dimensional (3D) host frameworks composed of the tetrel encapsulate the A guests within cages, adopt a crystal structure that closely resembles those of gas hydrates. A large group of binary, ternary, and even quaternary intermetallic compounds share the same type of crystal structure, originally observed for chlorine hydrate, which is known as the clathrate-I type.[7] Along with the intermetallic clathrates-I, there is also a group of clathrates-I with the reversed host–guest polarity,[8] in which halide or telluride anions balance a positively charged framework, which is again based on tetrels but with the addition of pnictogens or tellurium. Despite the structural similarity, these clathrates-I exhibit specific structural features, such as vacancy formation, deviation from cubic symmetry, and superstructure formation, as well as a variety of physical properties, including glass-like thermal conductivity.[9] The clathrate-I structure type provides quite a number of opportunities for varying the composition and the vacancy concentration, which seems to be necessary for enhancing the thermoelectric efficiency. Therefore, comprehension and delineation of the structure–property relationships for these clathrate-like compounds is a key requirement for the development of novel thermoelectric materials.

Herein, we report the synthesis of a new clathrate compound with reversed host–guest polarity, $Sn_{20.5}As_{22}I_8$, in which vacancy formation gives rise to a new $2\times2\times2$ superstructure of the clathrate-I type. We have investigated $Sn_{20.5}As_{22}I_8$ by means of X-ray diffraction, electron microscopy, Mössbauer spectroscopy, and by measurements of magnetic susceptibility, thermal and electrical conductivity, and thermopower. In particular, a very low thermal conductivity is reported for $Sn_{20.5}As_{22}I_8$.

Results and Discussion

Composition and X-ray powder data: We have shown previously that the composition of cationic type-I clathrates based on tin conforms to the Zintl–Klemm concept.[8–13] For clathrates with a cationic framework, this means that four electrons per framework atom or vacancy and one electron for each guest halogen atom are required. In this sense, a hypothetical $[Sn_{24}P_{22}]$ framework contains 22 excess electrons, as each phosphorus atom contributes five electrons. Eight of these electrons are transferred to iodine, and the remaining 14 electrons are compensated by removing 14/5 = 2.8 phosphorus atoms, leading to the composition $Sn_{24}P_{19.2}\square_{2.8}I_8$, which is in good agreement with the observed composition of $Sn_{24}P_{19.3(2)}\square_{2.7(2)}I_8$.[10] In the Sn-As-I system, the formation of a clathrate-I-type compound is also observed, but all attempts to obtain $Sn_{24}As_{19.3}\square_{2.7}I_8$ with the vacancies at the arsenic positions have been unsuccessful.[10] Thus, in this work, we have assumed that the vacancies occur at the tin sites. According to the Zintl concept, 14 residual electrons of the ideal $[Sn_{24}As_{22}]$ framework can be compensated by removing 14/4 = 3.5 tin atoms, leading to a clathrate-I compound with the composition $Sn_{20.5}\square_{3.5}As_{22}I_8$, which is indeed what we have observed in our experiments. A sample with a starting composition of $Sn_{20.5}As_{22}I_8$ was synthesized by means of an ampoule technique. The Sn/As/I ratio of the sample, as assessed by EDXS analysis, was found to be 40(1):45(1):14.8(4), which is in good agreement with that of 40.6:43.6:15.8 calculated for $Sn_{20.5}As_{22}I_8$. The composition of the new cationic clathrate-I $Sn_{20.5}\square_{3.5}As_{22}I_8$ is in full accord with the Zintl electron-counting scheme.

X-ray analysis of the sample after two-step annealing showed the presence of only one low-intensity peak ($I<1\%$ of the strongest peak) due to SnAs. The majority of diffraction peaks in the X-ray powder pattern could be indexed in the cubic system with a primitive unit-cell parameter of a_0 = 11.092(1) Å, which is typical for clathrate-I compounds. However, indexing of all weak reflections, except for one belonging to SnAs, was only possible in an F-cubic system by doubling the unit-cell parameter (Figure 1). The value

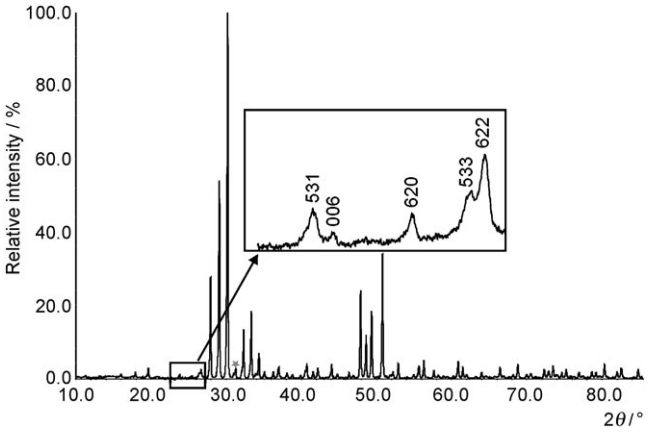

Figure 1. X-ray pattern of $Sn_{20.5}\square_{3.5}As_{22}I_8$ after the second annealing. The inset shows an enlarged portion of the pattern including the representative peaks with odd Miller indices. The unique observed reflection of SnAs is marked with an asterisk.

a = 22.1837(4) Å was obtained from least-squares fits, confirming the formation of a $2\times2\times2$ superstructure from the clathrate-I structure type by doubling the unit-cell parameter and a simultaneous change from a primitive to a face-centered cubic lattice. The same value, albeit with lower accuracy, was obtained for the sample after the first annealing; the lower accuracy can be attributed to the non-equilibrium state of the sample.

Crystal structure determination: Examination of systematic absences in the single-crystal X-ray data set (a = 22.1837(4) Å) suggested possible space groups as $F23$, $Fm\bar{3}$, $F432$, $F\bar{4}3m$, and $Fm\bar{3}m$. All reflections with odd Miller indices (superstructure reflections) were of very low intensity. Thus, in the first step, the structure was solved by using the

reflections of the primitive lattice with a unit-cell parameter of 11.092(1) Å, typical for clathrate-I compounds, and the space group $Pm\bar{3}n$ (no. 223) ($R_{int}=7.4\,\%$). All atomic positions of the ideal clathrate-I structure were located by direct methods. The 2*a* and 6*b* positions of the guest atoms were occupied by iodine, the 6*c* and 16*i* positions were set as arsenic, and the 24*k* position was set as tin, in analogy with the crystal structure of $Sn_{24}P_{19.3}I_8$.[10] Analysis of the difference Fourier map revealed four maxima lying close (ca. 0.60 Å) to the 6*c* arsenic position, As1, and three maxima near (ca. 0.57 Å) the 16*i* position of As2 (Figure 2a and b).

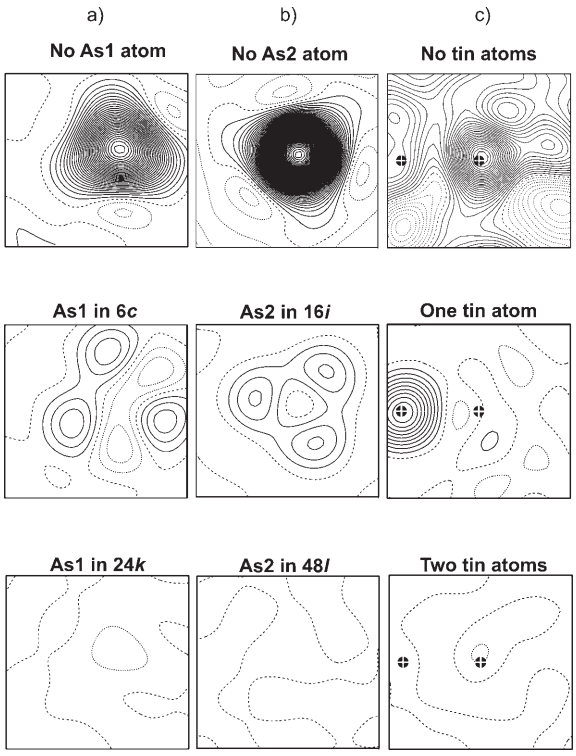

Figure 2. Difference electron density diagrams for $Sn_{20.5}\square_{3.5}As_{22}I_8$. The isolines (positive, solid; negative, dashed) are drawn at increments of 2 e Å^{-3}, and the frame size is 2×2 Å: a) difference electron density in the plane containing one edge of a tetrahedron formed by the As1 atoms; the ideal position of As1 is ≈0.1 Å off-plane; b) difference electron density in the plane containing a triangle formed by the As2 atoms; the ideal position of As2 is in the center of the picture; c) difference electron density near the positions of atoms Sn31, right cross, and Sn32, left cross; a cut with $z=0$ is shown.

For further refinement, As1 and As2 were shifted to the respective 24*k* and 48*l* positions, and their occupancy factors were set as $^1/_3$ and $^1/_4$, respectively. These values did not change upon refinement and were fixed during the final stages of the refinement in order to avoid severe parameter correlations. Analysis of the difference Fourier map revealed no remaining density at the 6*c* and 16*i* positions. It was also found that the occupancy factors for both iodine positions did not deviate from unity. A splitting of the 24-fold tin site into two partially occupied sites, Sn31 and Sn32, was observed (Figure 2c). The Sn31 to Sn32 distance is only 0.84 Å, which implies that the presence of any of these atoms in its site causes a vacancy in the neighboring atom position. The occupancy factors for each tin position were refined independently; the sum of the occupancies of Sn31 and Sn32 turned out to be substantially less than unity. The final refinement converged at $R_1=0.057$ for the calculated composition $Sn_{20.6(1)}\square_{3.4}As_{22}I_8$. Crystallographic data and atomic parameters are presented in Tables 1 and 2, respectively. Salient interatomic distances are summarized in Table 3, and a view of the crystal structure is shown in Figure 3.

Table 1. Crystallographic data for $Sn_{20.6(1)}\square_{3.4}As_{22}I_8$.

chemical formula	$Sn_{20.6(1)}As_{22}I_8$
M_r	5108.45
space group	$Pm\bar{3}n$ (no. 223)
T [K]	295
cell parameter a [Å]	11.092(1)[a]
V [Å^3]	1364.7(3)
Z	1
λ [Å]	0.71073
ρ_{calcd} [g cm^{-3}]	6.223
μ [mm^{-1}]	27.04
R_1,[b] wR_2[c]	0.057, 0.121

[a] Guinier data. [b] $R_1=\Sigma||F_o|-|F_c||/\Sigma|F_o|$. [c] $wR_2=[\Sigma w(F_o^2-F_c^2)^2/\Sigma w(F_o^2)^2]^{1/2}$, $w=[\sigma^2(F_o^2)+B\cdot p]^{-1}$; $p=(F_o^2+2F_c^2)/3$; $B=82.2911$.

With the aim of obtaining a structure solution in the face-centered cubic supercell, we analyzed the splitting of the Wyckoff positions upon subgroup–supergroup transformation from the space group $Pm\bar{3}n$, corresponding to the ideal clathrate-I structure type.[6] This revealed two probable space groups, $Fm3$ and $F23$ ($R_{int}=4.0\,\%$). In the space group $Fm3$, all atomic positions could be found by means of direct methods. A further refinement revealed extreme anisotropy in the displacement parameters for all of the framework atoms. In addition, multiple peaks in the difference Fourier map were found close to each atomic position of the framework, leading to a significantly high R value. A reduction in symmetry to the space group $F23$ did not remove these peaks. The best possible crystal structure solution obtained in the $F23$ space group had $R_1=16.6\,\%$, which cannot be

Table 2. Atomic coordinates, site occupancy factors (S.O.F.), and equivalent displacement parameters (U_{eq}) for $Sn_{20.6(1)}\square_{3.4}As_{22}I_8$.

Atom	Wyckoff	x/a	y/b	z/c	S.O.F.	U_{eq}[a]
I1	2*a*	0	0	0	1	0.0146(6)
I2	6*d*	$^1/_2$	0	$^1/_4$	1	0.0210(4)
As1	24*k*	0.2310(7)	0	0.480(1)	$^1/_4$	0.022(3)
As2	48*l*	0.195(5)	0.177(2)	0.190(7)	$^1/_3$	0.021(3)
Sn31	24*k*	0	0.3111(1)	0.1277(1)	0.714(8)	0.0196(4)
Sn32	24*k*	0	0.3256(8)	0.054(1)	0.144(6)	0.029(2)

[a] U_{eq} is defined as one-third of the trace of the orthogonalized U_{ij} tensor.

Table 3. Selected interatomic distances [Å] in the structure of $Sn_{20.6(1)}\square_{3.4}As_{22}I_8$.

Ranges of bond lengths within the framework	
Sn31–As2	2.49(7)–2.71(2)
Sn31–As1	2.59(1)–2.626(5)
Sn32–As1	2.60(1)–3.08(1)
Sn32–As2	2.92(8)–3.11(1)
Sn31–Sn31	2.832(3)
As2–As2	2.407(8)–2.422(8)
Short distances resulting from the splitting of the framework positions	
Sn31–Sn32	0.84(1)
Sn31–Sn32	2.02(1)
Sn31–As1	2.193(8)
Sn32–Sn32	1.19(2)
As1–As1	0.45(2)–0.53(1)
As2–As2	0.25(3)
Ranges of host–guest distances	
I1–As2	3.601(3)
I1–Sn32	3.659(9)
I1–Sn31	3.728(1)
I2–Sn32	3.432(5)
I2–Sn31	3.752(1)
I2–As1	3.780(6)–3.92(1)
I2–As2	3.97(3)–4.13(9)

considered as reliable. Thus, further analysis of the crystal structure was performed based on the subcell obtained in the space group $Pm\bar{3}n$.

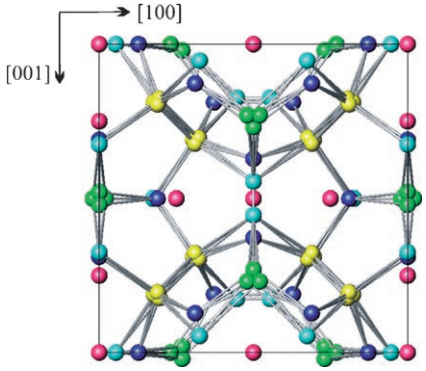

Figure 3. The subcell of the crystal structure of $Sn_{20.5}\square_{3.5}As_{22}I_8$. Iodine, purple; Sn31, light blue; Sn32 dark blue; As1, green; As2, yellow.

Description of the crystal structure: $Sn_{20.5}As_{22}I_8$ possesses a clathrate-I-type structure. The iodine atoms reside in the 2*a* and 6*d* positions of the $Pm\bar{3}n$ space group in the centers of 20- and 24-vertex polyhedral cages, respectively, which are formed in the framework composed of the tin and arsenic atoms (Figure 3). As a consequence of the splitting of the 24-fold tin position into two, Sn31 and Sn32, the Sn31 atoms are joined into pairs with an Sn–Sn separation of 2.84 Å. Each Sn31 atom is further bound to three arsenic atoms, thus completing its distorted-tetrahedral coordination. The Sn31–As distances fall in the range 2.49–2.71 Å, making them comparable with the Sn–As distances in another cationic clathrate based on tin and arsenic, $Sn_{19.3}Cu_{4.7}As_{22}I_8$ (2.54–2.85 Å).[8] Sn32 forms only three bonds to arsenic atoms and has one much longer interaction (3.43 Å) with iodine I2.

The separation between Sn32 and another tin atom, Sn31 or Sn32, is too short for a real covalent bond (2.02 or 1.2 Å); therefore, Sn32 does not form homonuclear bonds and its coordination is best described as involving three arsenic atoms plus one iodine atom in the second coordination sphere. Hence, if the Sn31 position is occupied, then another Sn31 is present in the adjacent position. If Sn32 is occupied, then the adjacent position is vacant. Therefore, the sum total of Sn31 and Sn32 atoms and vacancies in the 24*k* position should amount to 100%, which is in perfect agreement with the value of 100.2(6)% obtained by independent refinement of the occupancies of the Sn31 and Sn32 sites. Furthermore, the As1 and As2 atoms are not located in the ideal 6*c* and 16*i* positions, but are somewhat displaced. As2 is tetrahedrally coordinated by three tin atoms and one arsenic atom in another As2 position at a distance of 2.41 or 2.42 Å. As1 does not form any homonuclear bonds and is surrounded by four tin atoms. It should be noted that the presence of the vacancies at the tin sites implies that some of the As1 and As2 atoms have different coordination. However, the random distribution of the vacancies, coupled with the displacement of the arsenic atoms from their ideal positions, precludes further meaningful analysis of the coordination of the arsenic atoms.

For a clarification of the peculiarities of the crystal structure of the title compound, it is useful to compare the structure of $Sn_{20.5}\square_{3.5}As_{22}I_8$ with that of the phosphorus analogue, $Sn_{24}P_{19.3}\square_{2.7}I_8$ (Scheme 1). $Sn_{24}P_{19.3}I_8$ adopts the clathrate-I-type crystal structure, in which a positively charged framework built up of tin and phosphorus atoms traps guest iodine anions in large polyhedral cavities.[10] All atoms are located in their appropriate positions of the space group $Pm\bar{3}n$ corresponding to the clathrate-I type. The phosphorus atoms fully occupy the 16*i* position and partly occupy the 6*c* position. The 24*k* position is split into two partially occupied positions, Sn31 and Sn32, in a 55:45 ratio, evoking a different coordination of the tin atoms. Sn31 is four-coordinated by three phosphorus atoms and one tin atom, while Sn32 has 3+3 coordination in the form of a distorted octahedron, consisting of one tin atom and two phosphorus atoms at

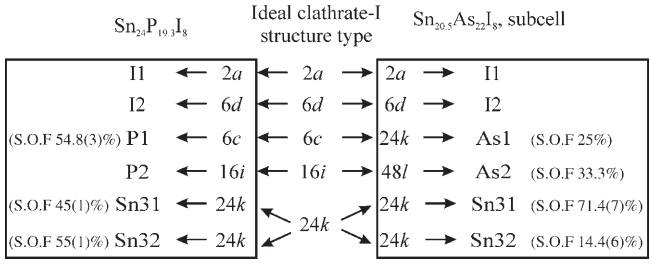

Scheme 1. Comparison of the site occupancy (S.O.F.: site occupancy factors) in $Sn_{24}P_{19.3}I_8$[10] and $Sn_{20.5}As_{22}I_8$; space group $Pm\bar{3}n$.

short distances plus three other Sn2 atoms at long distances ($d > 3.15$ Å). Distances between I2 in the larger cage and the atoms of the framework exceed 3.60 Å in all cases. On the contrary, in the crystal structure of $Sn_{20.5}As_{22}I_8$, vacancies are formed in the tin positions, as a result of which the Sn32 atom forms only three heteroatomic covalent bonds and has one iodine atom at a distance of 3.43 Å, which is much shorter than the typical distances between the guest iodine atoms and the host framework atoms observed in the crystal structure of $Sn_{24}P_{19.3}I_8$.

Mössbauer spectroscopy: The existence of two tin positions with different environments in $Sn_{20.5}As_{22}I_8$ has been confirmed by using ^{119}Sn Mössbauer spectroscopy. The spectrum is best fitted as a superposition of two doublets with the following hyperfine parameters (δ isomer shift, Δ quadrupole splitting) and absorption (A) (Figure 4): first doublet: $\delta =$ 2.23(1) mm s^{-1}, $\Delta = 0.66(1)$ mm s^{-1}, $A = 87(1)$ %; second doublet: $\delta = 2.92(4)$ mm s^{-1}, $\Delta = 1.52(7)$ mm s^{-1}, $A = 13(1)$ %. The doublet intensities are consistent, within experimental error, with the distribution of tin atoms over the aforementioned two sites of the crystal structure of $Sn_{20.5}As_{22}I_8$, 83(2) and 17(2) %, corresponding to crystallographic occupancies of 0.714(8) and 0.144(6) for the Sn31 and Sn32 positions, respectively. The first component of the spectrum can be attributed to the four-coordinated tin atom Sn31, which is bonded to three arsenic atoms and one tin atom. The isomer chemical shift and quadrupole splitting of the first doublet are very close to those reported for $Sn_{19.3}Cu_{4.7}As_{22}I_8$ ($\delta =$ 2.12 mm s^{-1}, $\Delta = 0.61$ mm s^{-1}),[8] which may be attributed to the fact that the four-coordinated tin has similar 1 Sn+3 As coordination. The noticeably large values of the quadrupole splitting and isomer shift for the second component reflect the coordination of Sn32, which is bonded to three arsenic atoms and has one iodine atom at a distance of 3.43 Å. The high isomer shift for the second component indicates a higher *s*-orbital contribution to the environment of the Sn32 atom. However, the noticeably large value of the quadrupole splitting ($\Delta = 1.52(7)$ mm s^{-1}) most likely reflects the 3+1 coordination of the Sn32 atom and corresponds to the axial asymmetry of the valence orbitals, which typically leads to an increased quadrupole splitting.

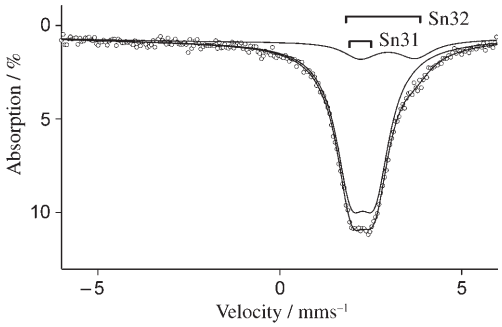

Figure 4. ^{119}Sn Mössbauer spectrum for $Sn_{20.5}\square_{3.5}As_{22}I_8$. Lines show the fitting doublets, brackets show the location of the doublets.

Superstructure and ordering models: Electron diffraction (ED) patterns for $Sn_{20.5}As_{22}I_8$ along the main zones are shown in Figure 5. The patterns could only be indexed in a cubic unit cell having a parameter twice as large as that of the type-I clathrate ($a \approx 22$ Å $\approx 2 \times a_0$). The ED pattern along [−111]* indicates the presence of a threefold axis running along the main diagonal of the cubic unit cell. No additional systematic extinctions, except those corresponding to the face-centered cubic lattice, were observed. Fourier transform (FT) of the HREM images for the [011] orientation resulted in the pattern shown in the upper-left corner of Figure 6. Comparing the FT and the ED patterns, one can see that superstructure spots corresponding to the *F* lattice are present in the FT pattern, which can only be completely indexed in a face-centered cubic space group, in good agreement with the experimental [011]* ED pattern (Figure 6). On the contrary, a computer simulation (not shown) based on the $Pm\bar{3}n$ space group, corresponding to the ideal clathrate-I structure with all atoms residing in their appropriate positions, does not fit the observed pattern.

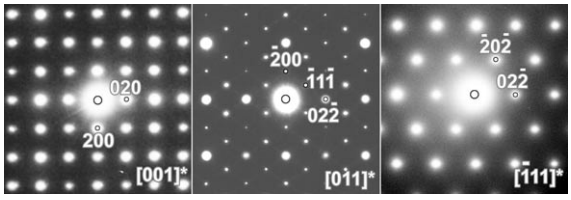

Figure 5. ED patterns along the major zones of $Sn_{20.5}\square_{3.5}As_{22}I_8$.

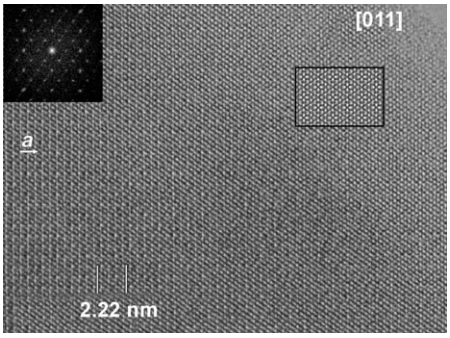

Figure 6. HREM image of $Sn_{20.5}As_{22}I_8$ along [011]. The FT pattern is shown in the upper-left corner. A simulated image ($T = 30$ Å, $\Delta F =$ 100 Å), calculated on the basis of the crystal structure refinement on the superstructure cell, is shown in the upper-right corner.

The ED study and HREM investigation of $Sn_{20.5}As_{22}I_8$ thus confirmed the presence of a superstructure ordering, resulting in a doubling of the unit-cell parameter and a change of the space group from $Pm\bar{3}n$ to either $F23$, $Fm\bar{3}$, $F432$, $F\bar{4}3m$, or $Fm\bar{3}m$. Nevertheless, all attempts to refine

the crystal structure in this doubled unit cell and the listed space groups using X-ray data led to strong disorder in the tin and arsenic positions and high *R* values. Each tin position obtained during the refinement exhibited the same type of splitting as in the substructure cell. In order to shed some light on this problem, an HREM study was performed. First, possible ways in which the tin atoms could be ordered in the superstructure unit cell were evaluated. For this, the atom positions obtained from the structure refinement on the substructure unit cell were transformed into a face-centered unit cell with doubled parameters. It was observed that the arrangement of atomic positions in the superstructure cell fitted the symmetry of the space groups $Fm\bar{3}$ or *F*23, whereas a transformation from space group $Pm\bar{3}n$ to *F*432, $F\bar{4}3m$, or $Fm\bar{3}m$ was impossible. It should be noted that neither the *F*23 nor the $Fm\bar{3}$ space group represents the maximal non-isomorphic subgroup of the space group $Pm\bar{3}n$ according to the International Tables for Crystallography.[14] These group–subgroup relations can only be described as a combination of "klassengleich" (class-equivalent) and "translationengleich" (lattice-equivalent) symmetry reductions.[15] The corresponding group relations and the transformation of the Wyckoff positions are shown in Scheme 2.

The space group *F*23 was chosen for the construction of ordering models as it is the less symmetric one. As mentioned above, in the substructure unit cell, two close-lying tin atoms, Sn31 and Sn32, occupy the 24*k* position of the space group $Pm\bar{3}n$. Transformation to the superstructure unit cell transfers each tin position into four 48*h* positions of the space group *F*23, hence giving rise to eight positions for the tin atoms (Table 4). The title compound has a composition close to $Sn_{21}\square_3As_{22}I_8$, which comprises 75% Sn31 atoms, 12.5% Sn32 atoms, and 12.5% vacancies in the 24*k* tin position of the subcell; therefore, four possible types of tin ordering may exist in the supercell. Analysis of the obtained atomic positions shows that the tin atoms have almost the same coordination as they do in the substructure unit cell. Each of the following combinations of tin positions in the superstructure cell may be present: i) Sn31a, Sn31b, Sn31c, Sn32d; ii) Sn31a, Sn31b, Sn32c, Sn31d; iii) Sn31a, Sn32b, Sn31c, Sn31d; iv) Sn32a, Sn31b, Sn31c, Sn31d (Table 4). In each ordering model, full occupancy can be assigned to the Sn31a, Sn31b, Sn31c, and Sn31d positions. At the same time, the Sn32a, Sn32b, Sn32c, and Sn32d positions should always have 50% occupancy, because each of them forms a pair of symmetrically equivalent positions lying at a physically unreasonable distance ($\approx$1 Å) from each other.

Table 4. Transformation of the tin atom positions during the transition from the subcell to the supercell.

Tin atom positions in a subcell ($Pm\bar{3}n$)					Tin atom positions in a supercell (*F*23)				
Atom	Pos.	*x*/*a*	*y*/*b*	*z*/*c*	Atom	Pos.	*x*/*a*	*y*/*b*	*z*/*c*
					Sn31a		0	0.1555	0.0639
					Sn31b		0	−0.1555	0.4361
Sn31		0	0.3111	0.1277					
					Sn31c		0.4055	1/4	0.1861
	24*k*					48*h*			
					Sn31d		0.5945	3/4	0.8139
					Sn32a		0	0.1628	0.0269
					Sn32b		0	−0.1628	0.4731
Sn32		0	0.3256	0.0538					
					Sn32c		0.4128	1/4	0.2231
					Sn32d		0.5872	3/4	0.7769

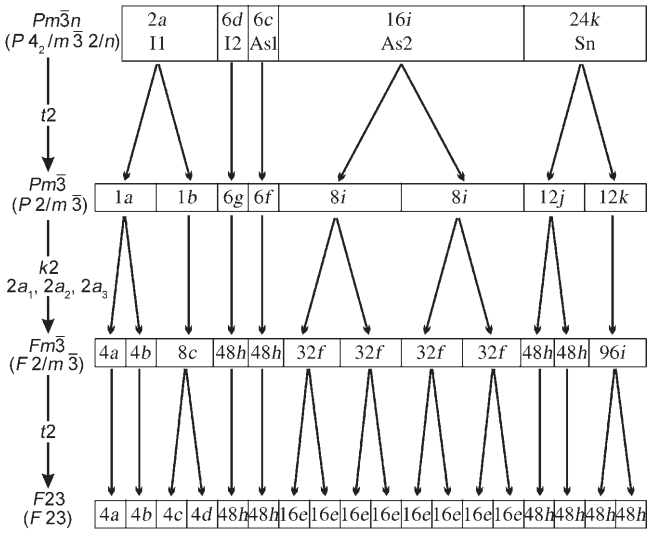

Scheme 2. Group–subgroup relationship for $Sn_{20.5}As_{22}I_8$ using the formalism of ref. [15] and splitting of the Wyckoff positions during the transformation from the ideal clathrate-I space group $Pm\bar{3}n$ to the *F*23 and $Fm\bar{3}$ space groups.

It should be noted that no reasonable way of ordering the arsenic atoms was found in the superstructure cell, and so these atoms were placed in their "ideal" positions as taken from their "ideal" positions 6*c* and 16*i* in the substructure unit cell according to Scheme 1. Based on the models obtained, HREM computer image simulations were performed. The simulated images along [011] appear to be very similar for all four models and do not differ significantly from the image calculated for the disordered crystal structure refined in the supercell. The information along the [001] orientation is more useful and is reproduced in the lower-right corner of Figure 7. One can see that ordering of the tin atoms results in fine changes in the contrast. The ordering results in the transformation of two bright dots, indicated by arrow I, into a diffuse line, indicated by arrow II. Careful examination of the HREM images obtained for thin crystallites reveals that the ordering of the tin atoms really exists (Figure 7, bottom left). However, it appears to be impossible to distinguish between the ordering models presented here. Figure 8 shows projections on the [001] plane for the four ordering models. In this projection, all four of the

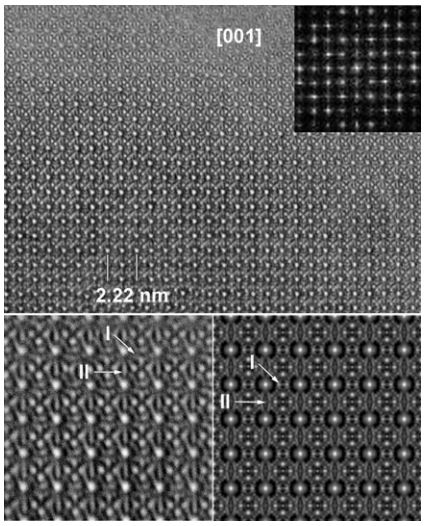

Figure 7. HREM image of $Sn_{20.5}\square_{3.5}As_{22}I_8$ along [001]. Bottom left, an enlargement of the HREM image; bottom right, a simulated image for an ordered model ($T=75$ Å, $\Delta F=-750$ Å); fine changes in contrast that appear due to the ordering of tin atoms are indicated by arrows.

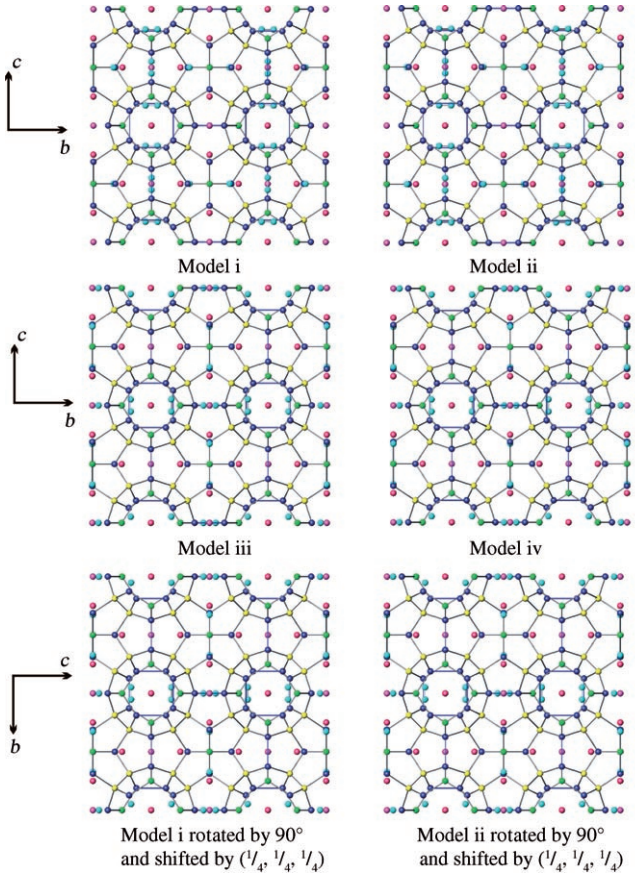

Figure 8. Ordering models of the crystal structure of $Sn_{20.5}\square_{3.5}As_{22}I_8$ in the space group $F23$. Projections on the [001] plane. The color code is the same as for Figure 3.

models look similar if two of them, (i) and (ii), are rotated through 90° and all atom positions are shifted by ($^1/_4$, $^1/_4$, $^1/_4$). Thus, the only difference for HREM imaging of the different ordering schemes is the 90° rotation. In practice, all ordering models may be simultaneously present in a crystallite. As reflected in Figure 9, some of the HREM images

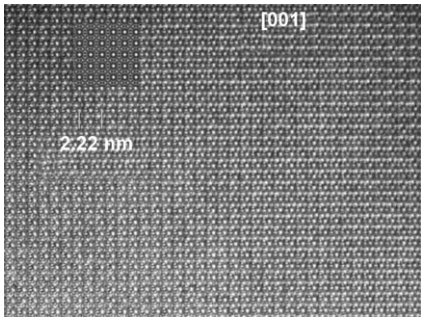

Figure 9. HREM image of $Sn_{20.5}\square_{3.5}As_{22}I_8$ along [001]. A computer-simulated image, based on the structure refinement in the supercell, space group $F23$ ($T=75$ Å, $\Delta F=-750$ Å), is inserted in the upper-left corner.

along [001] correspond to the simulated images obtained by using a disordered model refined in the supercell space group $F23$. This suggests an overlap of different types of ordered domains. We consider that intergrowth of randomly distributed small domains with different types of tin ordering is the reason why the crystal structure could not be reliably refined in the superstructure cell.

It should be stressed that the basic motif of the crystal structure is the same for all of the ordering models and therefore no domain boundaries are observed by HREM. Two points should be considered. First, the ordering in the space group $Fm\bar{3}$ will give a similar picture as in the space group $F23$, but with only two possible ordering variants. The 24*k* position of the $Pm\bar{3}n$ subgroup transforms into one 96*i* and two 48*h* positions in the space group $Fm\bar{3}$ (Scheme 2). Consequently, the Sn32 atoms can occupy only one of the 48*h* positions, leading to solely two possible ordering variants. The second important point is that, as mentioned above, all ordering models have been calculated for the composition $Sn_{21}\square_3As_{22}I_8$, assuming that the occupancy of the 24*k* position in the subcell is 75% Sn31 atoms, 12.5% Sn32 atoms, and 12.5% vacancies (the sum of the three-coordinated tin atoms and vacancies is exactly one-quarter (25%) of the total amount of tin atoms). However, the experimentally determined composition from the crystal structure solution in the subcell, which is in perfect agreement with the Zintl formalism, is $Sn_{20.6(1)}\square_{3.4(1)}As_{22}I_8$ (71.4(6)% Sn31 atoms, 14.4(6)% Sn32 atoms, and 14.2(6)% vacancies in the 24*k* tin position in the subcell). Thus, the total amount of vacancies and, consequently, the amount of three-coordinated tin atoms should be more than one-quarter of all tin atoms, namely 28.6%. For the ordered models, the "excess" vacancies (1.7%) should be somehow distributed over those three 48*h* tin positions of the $F23$ space group for which we initially assumed full occupancy. This leads us to the conclusion that a complete ordering of the tin atoms is not possible, even in the space group $F23$. These "excess"

vacancies in the tin atom positions may be an additional factor in facilitating the intergrowth of differently ordered domains.

Other types of clathrate-I superstructure have been reported in the literature.[11,16–18] Full ordering of the vacancies is observed in Ba_8Ge_{43},[16] in which the number of vacancies strictly corresponds to the multiplicity of the Wyckoff position in the superstructure space group $Ia\bar{3}d$. In Rb_8Sn_{44}[17] and $Sn_{14}In_{10}P_{21.2}I_8$,[11] partial ordering of the vacancies is associated with partial occupancies of various atomic positions in the space groups $Ia\bar{3}d$ and $P4_2/m$, respectively. However, in both cases, the crystal structures were successfully solved in the superstructure space group.

Magnetic and transport properties: $Sn_{20.5}As_{22}I_8$ possesses the typical physical properties of a Zintl phase;[19] it is a low-gap semiconductor and a diamagnet. Measurements of the temperature dependence of the magnetic susceptibility in high external magnetic fields (Figure 10) have revealed the diamagnetic behavior of $Sn_{20.5}As_{22}I_8$. The increase in $\chi(T)$ towards low temperatures may be attributed to traces of paramagnetic impurities, which are negligible at 300 K. The very weak dependence of the susceptibility upon the external magnetic field over the whole temperature range possibly stems from traces of ferromagnetic impurities.

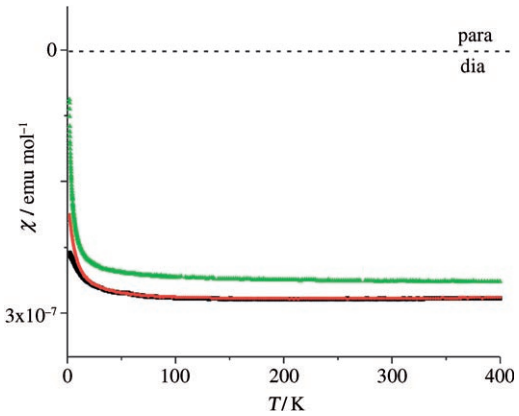

Figure 10. Molar magnetic susceptibility as a function of temperature for $Sn_{20.5}\square_{3.5}As_{22}I_8$: ▲ = 0.2 Tesla; ● = 3.5 Tesla; ■ = 7.0 Tesla.

$Sn_{20.5}As_{22}I_8$ exhibits a semiconductor-like temperature dependence of its electrical resistivity, $\rho(T)$. The results of electrical conductivity measurements carried out by two different methods, using hot-pressed and spark plasma sintering (SPS)-prepared samples, gave slightly different values of the room-temperature resistivity. The most reliable result, 1.05 Ω m, was obtained by means of standard *dc* four-probe measurements. However, the values of the band gap width estimated from fitting of the linear part of the dependences $\ln(1/\rho)$ versus $1/T$ in the temperature range 220–380 K are very close for both of these measurements and amount to 0.45 eV. The room temperature value of the Seebeck coefficient is $-180\ \mu V\,K^{-1}$.

The value of the band gap, 0.45 eV, is an order of magnitude larger than that of $Sn_{24}P_{19.3}I_8$.[10] According to band structure calculations on $Sn_{24}P_{19.3}I_8$,[11] it is mainly the orbitals of the 3+3-coordinated Sn atoms that contribute to the levels close to the Fermi level and therefore determine the transport properties. In the crystal structure of $Sn_{20.5}As_{22}I_8$, one type of tin atom is tetrahedrally coordinated, while the other forms only three bonds and has one more distant (3.43 Å) iodine atom in its second coordination sphere; therefore, there are no 3+3-coordinated tin atoms in the crystal structure of $Sn_{20.5}As_{22}I_8$, which is probably the reason for the substantial increase in the band gap.

Thermal conductivity: The thermal conductivity of $Sn_{20.5}As_{22}I_8$ as a function of temperature is shown in Figure 11. The temperature dependence of the thermal conductivity is characteristic of a semiconductor. It exhibits a maximum at about 70 K and then reaches a minimum at 210 K. The minimum value of about $0.4\ W\,m^{-1}\,K^{-1}$ at 210 K is, to the best of our knowledge, the lowest value ever reported for a low-gap semiconductor,[20–24] including various clathrates.[24] Some increase upon further increasing temperature is attributed to radiation losses. The measured room-temperature value, $\kappa \approx 0.5\ W\,m^{-1}\,K^{-1}$, though affected by radiation losses, is three times lower than the typical value for commercially used thermoelectric alloys based on Bi_2Te_3. The total thermal conductivity is the sum of the lattice thermal conductivity, κ_L, and the electronic thermal conductivity, κ_e; the latter can be estimated by using the Wiedemann–Franz law, $\kappa_e = \sigma \cdot L \cdot T$, in which $L = 2.45 \times 10^{-8}\ W\,\Omega\,K^{-2}$ is the Lorenz constant.[25] In the case of $Sn_{20.5}As_{22}I_8$, the resistivity is too high, and the contribution of κ_e to the total thermal conductivity is negligible. It should be noted that the moderate value of the Seebeck coefficient and especially the poor electrical conductivity lead to very low values (about 2×10^{-5}) of the thermoelectric efficiency (ZT) at room temperature.

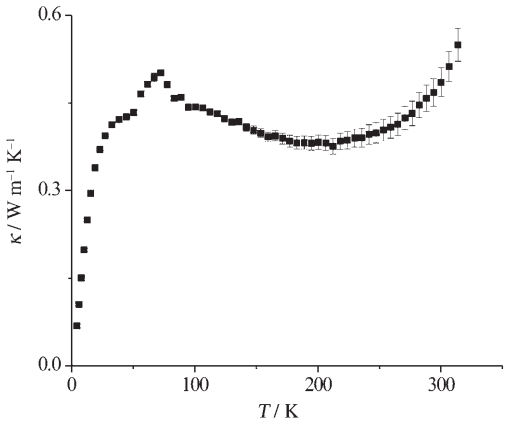

Figure 11. Thermal conductivity of $Sn_{20.5}\square_{3.5}As_{22}I_8$ as a function of temperature.

A comparison of the thermoelectric properties of $Sn_{20.5}As_{22}I_8$ and $Sn_{24}P_{19.3}I_8$ (preliminary investigation[26]) shows that the latter compound displays twofold higher thermal conductivity, a similar Seebeck coefficient, and a three-orders-of-magnitude higher electrical conductivity, which together lead to a moderate value of $ZT=0.02$ at room temperature. Further comparison shows that the guest atoms in $Sn_{24}P_{19.3}I_8$ may have more space in which to "rattle", because the host–guest distances are about 0.2 Å longer than those in $Sn_{20.5}As_{22}I_8$, and the atomic displacement parameters for the iodine guest atoms are practically the same in both crystal structures.[10] Typically, the "rattling" of guest atoms is considered to be the main reason for phonon scattering[27] and, consequently, low thermal conductivity. However, comparison of these two compounds does not point to a preferable "rattling" of the guest atoms in either of the crystal structures. We argue, therefore, that "rattling" is by no means the only mechanism by which phonon scattering can occur. The low thermal conductivity is attributed to a high degree of disorder,[28] which, for clathrate-like compounds, includes a splitting of the sites, mainly those of the guest atoms.[29] In $Sn_{20.5}As_{22}I_8$, the degree of disorder is indeed very high. It is manifested in a random distribution of vacancies, a splitting of the tin atom positions, a shift of the arsenic atoms from their ideal positions, and the intergrowth of small, randomly distributed and differently ordered domains. We attribute the abnormally low thermal conductivity of $Sn_{20.5}As_{22}I_8$ to the high degree of disorder of the crystal structure rather than to the often discussed "rattling" of the guest atoms.

Conclusion

$Sn_{20.5}As_{22}I_8$ is a new ternary cationic clathrate-I derivative. It exhibits a new type of $2\times2\times2$ superstructure resulting from the partial ordering of vacancies and two different kinds of tin atoms in the cationic framework. The bulk compound is not uniform and can be described as an intergrowth of randomly distributed small domains with different types of ordering. $Sn_{20.5}As_{22}I_8$ is a diamagnet and a semiconductor with an estimated band gap of 0.45 eV. It displays abnormally low thermal conductivity, with a room temperature value of 0.5 $W m^{-1} K^{-1}$, which is attributed to a high degree of disorder in the crystal structure.

Experimental Section

Sample preparation: $Sn_{20.5}As_{22}I_8$ was prepared by means of a two-step standard ampoule synthesis. All preparations were carried out in an argon-filled glove box (O_2 content <1.2 ppm, H_2O content <1 ppm), which was also used to store the starting materials. Finely dispersed powders of metallic tin (Chempur, 99.99%) and tin(IV) iodide (Alfa, 99.998%) and pieces of arsenic (Chempur, 99.999%) were used as received. The pieces of arsenic were first mechanically reground in an agate mortar. The appropriate stoichiometric amounts of tin and tin(IV) iodide were then added, and all three components were mixed together. The powder thus obtained was pressed into a pellet and sealed in a silica tube under vacuum and then annealed at 775 K for five days. After regrinding and subsequent pressing, the sample was subjected to a second annealing in an evacuated sealed silica tube at 675 K for ten days. After the second annealing and regrinding, the sample was obtained as a black, air- and moisture-stable, homogeneous powder. For X-ray diffraction analysis, a single crystal of $Sn_{20.5}As_{22}I_8$ was selected from the non-equilibrium reaction product after the initial annealing at 725 K for five days of the starting materials in an Sn/As/SnI_4 ratio of 17:22:2. Other routes for the preparation of single crystals were also used, including a melt technique, prolonged stoichiometric annealing, and chemical transport reactions, and most of them proved to be successful. In all cases, single crystals were tested by means of Laue photographs and preliminary data set collection, and although they were found to be of poorer quality, they had the same unit-cell parameter within the estimated standard deviation (esd).

For resistivity measurements, dense pills were prepared by spark plasma sintering (SPS). $Sn_{20.5}As_{22}I_8$ powder was treated at 573 K and 500 MPa for 1 h in an argon atmosphere using a WC die. For thermoelectric property measurements, the sample obtained after two-step annealing was hot-pressed at 553 K in an argon-filled glove box into pellets in the form of a parallelepiped (length 3.55 mm; cross-section 2.4 mm^2). To check for any possible decomposition, the sample was subjected to X-ray powder analysis after both the hot pressing and the SPS treatment; no change in the X-ray pattern was detected.

Sample characterization: The sample was characterized by means of X-ray powder and EDXS analyses. X-ray analysis was performed by using a Huber G670 image plate camera, $Cu_{K\alpha1}$ radiation, $\lambda=1.540598$ Å; the unit-cell parameters were calculated from least-squares fits using LaB_6 (cubic, $a=4.15692$ Å) as an internal standard, utilizing the program package WinCSD.[30] For EDXS analysis, the surface of a pill pressed after the second annealing was polished by standard methods and then examined with partly polarized light (ZEISS Axioplan2 optical microscope) using differential interference contrast. Elemental analysis was performed using a Philips XL30 scanning electron microscope.

Single-crystal X-ray diffraction experiment: A single crystal tested by means of Laue photographs was selected for single-crystal X-ray diffraction analysis, which was carried out on a Rigaku AFC7 four-circle diffractometer equipped with a Mercury CCD area detector. The data collection and refinement parameters are given in Table 1. SHELX-97 software was used for the crystal structure solution and refinement.[31] Further details of the crystal structure determination may be obtained from the Fachinformationszentrum Karlsruhe, D-76344 Eggenstein-Leopoldshafen, Germany, on quoting the depository number CSD-416531.

Mössbauer spectroscopy: The ^{119}Sn spectrum was recorded by using a conventional constant-acceleration Mössbauer spectrometer. The measurements were performed at 300 K with a $Ca^{119m}SnO_3$ source maintained at room temperature. Isomer chemical shifts were referenced to a $CaSnO_3$ absorber at 300 K.

Transmission electron microscopy: Electron diffraction (ED) patterns were obtained using a Philips CM20 microscope. High-resolution electron microscopy (HREM) investigations were performed using a JEOL 4000EX microscope operating at 400 kV. The sample for TEM was crushed, dispersed in methanol, and deposited on a carbon mesh grid. HREM images were simulated by using Mac Tempas and Crystal Kit software.

Physical property measurements: The magnetic susceptibility (χ) of $Sn_{20.5}As_{22}I_8$ was measured in external magnetic fields of 0.2, 3.5, and 7.0 Tesla over the temperature range 2–400 K using a superconducting quantum interference device (SQUID) magnetometer (MPMS XL-7, Quantum Design). The powder sample was contained in a pre-calibrated quartz tube. Corrections for the sample container were applied.

Simultaneous measurements of the Seebeck coefficient, thermal conductivity, and electrical resistivity were performed using a Quantum Design Physical Property Measurement System (PPMS) equipped with a thermal transport option. Additional resistivity measurements were carried out by means of a standard *dc* four-point method between 3.8 and 320 K. A parallelepiped of approximate dimensions $1\times1\times5$ mm was cut from the

SPS-prepared sample. Contacts on the sample were fixed with a silver-filled epoxy paste.

Acknowledgements

The authors thank Dr. N. Reinfried for the SPS treatment of the samples, Dr. U. Burkhardt for performing the EDX analyses, R. Koban for help with the physical property measurements, and Dr. A. M. Abakumov for fruitful discussions. A. V. O. thanks the Belgian Federal Science Policy Office for a research fellowship. This work has been supported by the Russian Foundation for Basic Research and the European Commission 5th Framework Program.

[1] G. A. Slack, in *CRC Handbook of Thermoelectrics* (Ed.: D. M. Rowe), Chemical Rubber Co., Boca Raton, FL, **1995**.
[2] B. S. Sales, D. Mandrus, R. K. Williams, *Science* **1996**, *272*, 1325–1328.
[3] G. S. Nolas, L. J. Cohn, G. A. Slack, S. B. Schujman, *Appl. Phys. Lett.* **1998**, *73*, 178–180.
[4] For filled scutterudites, see, for example: B. S. Sales, D. Mandrus, B. C. Chakoumakos, V. Keppens, J. R. Thompson, *Phys. Rev. B* **1997**, *56*, 15081–15089.
[5] S. Paschen, W. Carrillo-Cabrera, A. Bentien, V. H. Tran, M. Baenitz, Yu. Grin, F. Steglich, *Phys. Rev. B* **2001**, *64*, 214404, and references therein.
[6] J. S. Kasper, P. Hagenmuller, M. Pouchard, *Science* **1965**, *150*, 1713–1714.
[7] A. F. Wells, *Structural Inorganic Chemistry*, 5th ed., Clarendon, Oxford, **1986**, chapter 15.
[8] K. A. Kovnir, A. V. Sobolev, I. A. Presniakov, O. I. Lebedev, G. Van Tendeloo, W. Schnelle, Yu. Grin, A. V. Shevelkov, *Inorg. Chem.* **2005**, *44*, 8786–8793, and references therein.
[9] K. A. Kovnir, A. V. Shevelkov, *Russ. Chem. Rev.* **2004**, *73*, 923–938.
[10] M. M. Shatruk, K. A. Kovnir, A. V. Shevelkov, I. A. Presniakov, B. A. Popovkin, *Inorg. Chem.* **1999**, *38*, 3455–3457.
[11] M. M. Shatruk, K. A. Kovnir, M. Lindsjö, I. A. Presniakov, L. A. Kloo, A. V. Shevelkov, *J. Solid State Chem.* **2001**, *161*, 233–242.
[12] K. A. Kovnir, J. V. Zaikina, L. N. Reshetova, A. V. Olenev, E. V. Dikarev, A. V. Shevelkov, *Inorg. Chem.* **2004**, *43*, 3230–3236.
[13] K. A. Kovnir, M. M. Shatruk, L. N. Reshetova, I. A. Presniakov, E. V. Dikarev, M. Baitinger, F. Haarmann, W. Schnelle, M. Baenitz, Yu. Grin, A. V. Shevelkov, *Solid State Sci.* **2005**, *7*, 957–968.
[14] *International Tables for Crystallography, Vol. A* (Ed.: T. Hahn), Kluwer, Dordrecht, **1989**, chapter 7, p. 672.
[15] H. Bärnighausen, *MATCH* **1980**, *9*, 139–175.
[16] W. Carrillo-Cabrera, S. Budnyk, Yu. Prots, Yu. Grin, *Z. Anorg. Allg. Chem.* **2004**, *630*, 2267–2276.
[17] F. Dubois, T. F. Fässler, *J. Am. Chem. Soc.* **2005**, *127*, 3264–3265.
[18] J. Dünner, A. Mewis, *Z. Anorg. Allg. Chem.* **1995**, *621*, 191–196.
[19] G. J. Miller, in *Chemistry, Structure, and Bonding of Zintl Phases and Ions* (Ed.: S. M. Kauzlarich), VCH, New York, **1996**, and references therein.
[20] G. S. Nolas, G. A. Slack, S. B. Schujman, in *Recent Trends in Thermoelectric Materials Research* (Ed.: T. M. Tritt), Academic Press, San Diego, **2001**.
[21] M. A. McGuire, T. K. Reynolds, F. J. DiSalvo, *Chem. Mater.* **2005**, *17*, 2875–2884.
[22] K. Ueno, A. Yamamoto, T. Noguchi, T. Inoue, S. Sodeoka, H. Takazawa, C. H. Lee, H. Obara, *J. Alloys Compd.* **2004**, *384*, 254–260.
[23] D.-Y. Chung, T. P. Hogan, M. Rocci-Lane, P. Brazis, J. R. Ireland, C. R. Kannewurf, M. Bastea, C. Uher, M. G. Kanatzidis, *J. Am. Chem. Soc.* **2004**, *126*, 6414–6428.
[24] A. Bentien, M. Christensen, J. D. Bryan, A. Sanchez, S. Paschen, F. Steglich, G. D. Stucky, B. B. Iversen, *Phys. Rev. B* **2004**, *69*, 045107.
[25] M. A. White, *Properties of Materials*, Oxford University Press, Oxford, **1999**.
[26] K. A. Kovnir, Doctoral dissertation, Moscow State University, Moscow, **2004**.
[27] B. B. Iversen, A. E. C. Palmqvist, D. E. Cox, G. S. Nolas, G. D. Stucky, N. P. Blake, H. Metiu, *J. Solid State Chem.* **2000**, *149*, 455–458.
[28] See: J. Nylen, M. Andersson, S. Lidin, U. Häusermann, *J. Am. Chem. Soc.* **2004**, *126*, 16306–16307.
[29] S. Paschen, V. Pacheco, A. Bentien, A. Sanchez, W. Carrillo-Cabrera, M. Baenitz, B. B. Iversen, Yu. Grin, F. Steglich, *Phys. B* **2003**, *328*, 39–43.
[30] L. G. Akselrud, P. Y. Zavalij, Yu. N. Grin, V. K. Pecharsky, B. Baumgartner, E. Wölfel, *Mater. Sci. Forum* **1993**, *133–136*, 335.
[31] a) G. M. Sheldrick, SHELXS-97, Program for crystal structure solution, University of Göttingen (Göttingen), Germany, **1997**; b) G. M. Sheldrick, SHELXL-97, Program for crystal structure refinement, University of Göttingen (Göttingen), Germany, **1997**.

Received: December 11, 2006
Published online: March 23, 2007

